

## Article

# Asbestos Bodies in Human Lung: Localization of Iron and Carbon in the Coating

Alessandro Croce <sup>1,2,\*</sup> , Giorgio Gatti <sup>3</sup> , Antonio Calisi <sup>2</sup> , Laura Cagna <sup>2</sup>, Donata Bellis <sup>4</sup> , Marinella Bertolotti <sup>1</sup>, Caterina Rinaudo <sup>2</sup>  and Antonio Maconi <sup>5</sup> 

- <sup>1</sup> SSD Research Laboratories, Research Training Innovation Infrastructure, Research and Innovation Department (DAIRI), Azienda Ospedaliero-Universitaria SS. Antonio e Biagio e Cesare Arrigo, Via Venezia 16, 15121 Alessandria, Italy; mbertolotti@ospedale.al.it
  - <sup>2</sup> Department of Science and Technological Innovation, University of Eastern Piedmont, Viale T. Michel 11, 15121 Alessandria, Italy; antonio.calisi@uniupo.it (A.C.); laura.cagna@uniupo.it (L.C.); caterina.rinaudo@uniupo.it (C.R.)
  - <sup>3</sup> Department for Sustainable Development and Ecological Transition, Piazza S. Eusebio 5, 13100 Vercelli, Italy; giorgio.gatti@uniupo.it
  - <sup>4</sup> Centre “G. Scansetti” Via Pietro Giuria 9, 10100 Turin, Italy; donata.bellis@libero.it
  - <sup>5</sup> Research Training Innovation Infrastructure, Research and Innovation Department (DAIRI), Azienda Ospedaliero-Universitaria SS. Antonio e Biagio e Cesare Arrigo, Via Venezia 16, 15121 Alessandria, Italy; amaconi@ospedale.al.it
- \* Correspondence: alessandro.croce@uniupo.it

**Abstract:** Asbestos is a term that includes six fibrous mineral phases related to different lung diseases, including asbestosis, lung cancer, and Malignant Pleural Mesothelioma (MPM). Since the last century, these minerals have been widely studied under their mineralogical/chemical and physical aspects with *in vivo* and *in vitro* studies to understand the mechanisms of their carcinogenicity. There are several techniques described in the literature, as optical and electron microscopies, for the identification of coated (asbestos bodies, ABs) and uncoated fibers, but only micro-Raman spectroscopy permits a sure characterization of these minerals—and of the related phases—directly in the histological sections of pulmonary parenchyma without any manipulation. In this case, the risk of the loss of associated inorganic phases from asbestos bodies (ABs) and fibers (e.g.: iron or carbonaceous micro-particles) is avoided. Asbestos bodies are produced by the activity of alveolar macrophages with degradation/inactivation of asbestos fibers. Inside the alveolar macrophages, organic and inorganic material settles on the foreign fibers forming an iron-rich proteic and carbonaceous coating. In this study, Variable Pressure Scanning Electron Microscopy with annexed Electron Dispersive Spectroscopy (VP-SEM/EDS) and micro-Raman spectroscopy were applied to the characterization of the phases in the ABs. Characterization of carbonaceous materials (CMs), observed in pristine asbestos phases in previous works, was therefore performed, addressing the micro-Raman laser beam on different points of the asbestos bodies, and Raman mappings on ABs were carried out for the first time. Coupling the data obtained by VP-SEM/EDS and micro-Raman spectroscopy, it was possible to collect information about the iron and carbonaceous phases adhered to the fibers, probably lost during the classical tissue digestion procedures. Information about both mineral and carbonaceous components might be useful to understand the whole structure of “asbestos bodies” and the inflammogenic and carcinogenic effects of the asbestos phases coupled to CMs, that might derive from cigarette smoke or from environmental pollution; this study might be useful to deepen also the possible detrimental role of ABs in the tissues.

**Keywords:** asbestos; histological sections; asbestos bodies; ferritin; carbonaceous material; micro-Raman spectroscopy



**Citation:** Croce, A.; Gatti, G.; Calisi, A.; Cagna, L.; Bellis, D.; Bertolotti, M.; Rinaudo, C.; Maconi, A. Asbestos Bodies in Human Lung: Localization of Iron and Carbon in the Coating. *Geosciences* **2024**, *14*, 58. <https://doi.org/10.3390/geosciences14030058>

Academic Editors: Jesus Martinez-Frias, Fedor Lisetskii and Maurizio Barbieri

Received: 30 October 2023  
Revised: 7 February 2024  
Accepted: 16 February 2024  
Published: 23 February 2024



**Copyright:** © 2024 by the authors. Licensee MDPI, Basel, Switzerland. This article is an open access article distributed under the terms and conditions of the Creative Commons Attribution (CC BY) license (<https://creativecommons.org/licenses/by/4.0/>).

## 1. Introduction

The term “asbestos” indicates six natural mineral fibers that are well known for their mechanical/chemical properties (e.g.: resistance to heat, corrosion, and electricity) and for their carcinogenic effect on human health [1,2]. These minerals are: (i) tremolite ( $\text{Ca}_2\text{Mg}_5[\text{Si}_8\text{O}_{22}](\text{OH})_2$ ), (ii) actinolite ( $\text{Ca}_2(\text{Mg},\text{Fe}^{2+})_5[\text{Si}_8\text{O}_{22}](\text{OH})_2$ ), (iii) anthophyllite ( $(\text{Mg},\text{Fe}^{2+})_7[\text{Si}_8\text{O}_{22}](\text{OH})_2$ ), (iv) cummingtonite-grunerite (amosite) ( $(\text{Fe}^{2+},\text{Mg})_7[\text{Si}_8\text{O}_{22}](\text{OH})_2$ ), (v) riebeckite (crocidolite) ( $\text{Na}_2\text{Fe}^{2+}_3\text{Fe}^{3+}_2[\text{Si}_8\text{O}_{22}](\text{OH})_2$ ), and (vi) chrysotile ( $\text{Mg}_3\text{Si}_2\text{O}_5(\text{OH})_4$ ). Among them, the first five are amphiboles (double-chain silicates), and the last one is a phyllosilicate belonging to the serpentine family [3–5].

These minerals have been extensively extracted and used in factories, in particular during the industrial expansion in the XX century: of the six phases, the most manufactured were chrysotile, crocidolite, and amosite asbestos. On the other hand, since the beginning of the last century, different researchers have highlighted more and more the evidence relating asbestos exposure to respiratory diseases—i.e., lung carcinoma, asbestosis, Malignant Pleural Mesothelioma (MPM) [6,7]—and also to tumors affecting other sites (e.g.: gastrointestinal or reproductive system) [1,8–15]. For this reason, these minerals have been studied not only under their mineralogical aspects but also with the goal to understand the carcinogenic properties and the fibrogenetic activities [16–31]. Many research studies have been addressed to define their structures, chemical compositions, and physical properties but often considering the raw bulk samples [5,24,27,31]. In the past and in recent years, more performing methodologies have been developed allowing a deeper characterization of the raw materials, also inside the lungs and/or other biological materials without the need for any manipulation of the samples [32–35].

Moreover, in the last years, the research community focused attention on the key point that is still unclear: the relationships between the mineralogical inorganic components and the biological medium, in particular in the fiber/cell contact surfaces [36–38]. Nevertheless, also in these studies, the samples underwent different manipulation procedures that can affect the samples themselves. So, there is still the need to carry out additional analyses using a technique that does not require sample preparation.

One of the methodologies allowing this kind of analysis is micro-Raman spectroscopy. This technique, thanks to the microscope annexed to the spectrometer, allows the characterization of the fibers in different areas and the identification of phases on their surfaces [34,35].

Croce et al., 2015, 2018, demonstrated that micro-Raman spectroscopy allows to characterize different iron compounds—goethite ( $\text{FeO}(\text{OH})$ ), hematite ( $\text{Fe}_2\text{O}_3$ ), and jarosite ( $\text{KFe}_3^{3+}(\text{SO}_4)_2(\text{OH})_6$ )—on erionite fiber surfaces [39] and carbonaceous materials (CMs) lying on standard samples of the three most manufactured asbestos phases—crocidolite, amosite, and chrysotile [34,35]. The technique highlighted, in an unequivocally way, the position of these phases, with a great advantage with respect to the methodologies requiring sample preparation (e.g.: X-ray diffraction, gas chromatography, UV spectrophotometry, IR, mass spectroscopy, and Scanning and Transmission Electron Microscopies) [40–48].

In this study, micro-Raman spectroscopy has been applied to the characterization of the phases composing asbestos bodies (ABs, coated asbestos fibers) [32] inside pulmonary histological sections of patients affected by MPM. ABs derive from the frustrated phagocytosis carried out by lung macrophages, which produce a deposition of minerals and iron proteins on fiber surfaces; this is due to fiber dimensional parameters (length  $\geq 5 \mu\text{m}$ , thickness  $\leq 3 \mu\text{m}$ , and length/thickness ratio  $> 3$ ) [11] that do not permit the fiber removal by the cells. These morphologies are typical markers of past asbestos exposures, and they represent a last attempt of the human body to isolate the fibers, but that might produce damage to the body itself. ABs are formed by an internal asbestos fiber (called “core”) and by a coating composed of iron-rich protein, mainly composed of ferritin containing the mineral ferrihydrite, acid mucopolysaccharides, phospholipids, and lung surfactant proteins (called “coating”) [36].

Rinaudo et al., 2010, demonstrated that micro-Raman spectroscopy is able to identify a crystallization of hematite from the iron-rich cores of the protein coating, under the power of

the 632.8 nm laser [49], considering the 1200–200  $\text{cm}^{-1}$  spectral range. The results obtained on asbestos bodies of different shapes will be presented, considering also the spectral range where organic fingerprints [34,35] lie, trying to understand if carbonaceous materials may be identified also in these biological materials. In this work, the goal will be the identification of other organic components, considering, in particular, the 1800–1200  $\text{cm}^{-1}$  spectral range, where the CM first-order bands lie, trying to understand if carbonaceous components are identifiable after AB formation.

In fact, during tissue digestion or sample preparation, it is possible to lose some organic or inorganic components of ABs, and the application of micro-Raman spectroscopy may be useful to observe and integrate the data obtained with other techniques. Moreover, it is possible to obtain Raman maps, visualizing where the different components are present, and a second goal of this work is to apply this methodology for the first time to understand also where the different phases in the ABs are localized.

Coupling the data obtained by applying this technique and SEM/EDS analyses may be useful for understanding the features from the chemical and spectroscopical points of view. In fact, the application of SEM/EDS directly on histological sections is useful to chemically identify the mineral fibers, also when they are covered by the iron-rich proteins: in this work, the method presented in Croce et al., 2013 [32], has been applied, with the aim of better understanding which iron is ascribable to the inorganic fiber.

The obtained data, both from the mineral phase and from the adhered particles on the iron-protein covering, might be useful for future studies in the field of asbestos-related diseases.

In fact, the first problem in asbestos fiber identification is the understanding of the mineral phase inside the covering, and future application—and improvement—of these non-destructive techniques might be useful in medical legal debates.

Secondly, the characterization and the localization of other phases located next to asbestos fibers or ABs might be useful to studies concerning the carcinogenic effects of the different particles. For example, keeping in mind that cigarette smoke has a synergistic effect with asbestos oncogenic consequences [36], in the future, a study analyzing a greater number of patients (or on in vivo or in vitro samples) might be useful to improve the knowledge of the mechanisms about the disease development.

So, the strict collaboration of geologists, geoscientists, and mineralogists, considered in this case as “medical geologists”, with other experts in different disciplines (e.g.: health sciences, pathology, epidemiology) might be useful to reach the goal aimed at eradicating or reducing the effects of the diseases and understanding the pathways to find long-term solutions [50].

## 2. Materials and Methods

Lung samples from one patient affected by MPM, diagnosed postmortem, were embedded in a paraffin block and then cut using a microtome into 5  $\mu\text{m}$  thick sections. The patient’s information was opportunely anonymized to the analysts. Because this study is an exploratory analysis and all the data were anonymized, no informed consent was obtained from the patient, and it was not necessary in accordance with our Ethical Committee, so the collection and inclusion in the analysis of the patient’s information on exposure and life history were not carried out. The sections were fixed on plastic slides in order to avoid interference between the chemicals composing the glass and the ones forming the fibrous materials contained inside the ABs. The slides were put in an oven at 60  $^{\circ}\text{C}$  overnight to degrade the paraffin film embedding the tissues. The sections were then observed under an Optical Microscope (OM), equipped with two polarizers, to identify the ABs, and their positions were defined by means of an x-y grid for further analyses, both by SEM/EDS and micro-Raman spectroscopy.

SEM/EDS analyses were performed using an ESEM Quanta 200 SEM (FEI Company, Hillsboro, OR, USA), equipped with an EDS (EDAX, Mahwah, NJ, USA). Back-scattered images (BSE), characterized by white/black contrasts produced by inorganic phases embedded inside the tissues, allowed easy identification of the silicate fibers [11,32]. The

experimental conditions were: pressure = 90 Pa, working distance = 10 mm, and accelerating voltage = 20 kV. EDS spectra were collected and processed using GENESIS software, v. 3.6. To determine the elemental composition of the observed inorganic phases, EDS micro-analyses were carried out following the procedure described in our previous works [11].

Raman analyses were carried out using a JobinYvon HR Evolution micro-Raman spectrometer (HORIBA JobinYvon, Paris, France), equipped with a 532 nm Nd:YAG laser source. Autocalibration of the spectroscope was performed fixing the  $\sim 520.6\text{ cm}^{-1}$  band of the Si reference sample before every experiment. The spectra were collected addressing 3.2% of the full laser power directly on the fiber embedded in the tissue; the spectra were acquired with 1 exposure of 100 s for each spectral range, under the 80x objective of the microscope coupled to the instrument. Employing this experimental set-up, well-resolved spectra and maps could be collected. Raman maps were recorded using the same parameters and rectangular areas, chosen on the basis of the AB morphologies, were analyzed in order to obtain images characterized by two-dimensional high resolutions.

Moreover, a fitting procedure has been applied to representative spectra, using the software Fytik v. 0.9.8, to define the order degree of the organic component adhered to the asbestos body. It was carried out considering six different components, one Gaussian and five Lorentzian, using a dedicated script described in Croce et al., 2021 [51]. The bands are called D1 (lying at about  $1330\text{ cm}^{-1}$ , deriving from defective carbons), G (about  $1550\text{--}1580\text{ cm}^{-1}$ , related to the extension of ordered regions), D2 (related to the D1 band, lying at about  $1600\text{--}1615\text{ cm}^{-1}$ ), D3 (the Gaussian one, at  $1450\text{--}1550\text{ cm}^{-1}$ ), D4 ( $1150\text{--}1230\text{ cm}^{-1}$ ), and D5 ( $1060\text{--}1120\text{ cm}^{-1}$ ). This process is necessary to obtain the best fit to calculate shapes and intensities of the bands in the  $800\text{--}1800\text{ cm}^{-1}$  range: in particular, the intensities of the D1 and G bands are important to calculate the  $R_1$  ratio, related to the disorder degree of the carbonaceous materials.

### 3. Results

Histological sections from an MPM patient were carefully studied under an OM to detect the presence of ABs and localize them in the tissues. As shown in Figure 1, they can be classified on the basis of their shape, color, and morphology. The observed ABs appeared dark or red/brown (Figure 1a,b), often surrounded by great areas of black aggregates (Figure 1c).

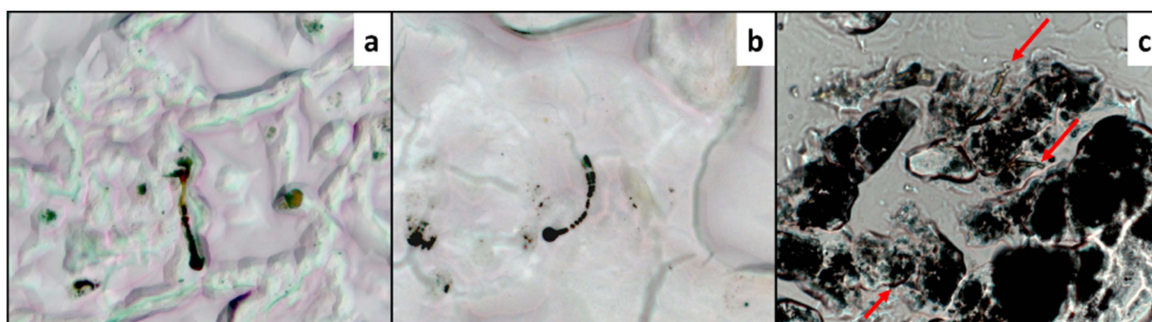


**Figure 1.** (a,b) Example of asbestos bodies observed in the patient's lung tissue and showing a dark color (magnification  $40\times$  in (a) and  $63\times$  in (b)); (c) Black aggregates near the ABs (arrows indicate some short fibers); magnification  $63\times$ .

A set of histological sections from the lung tissue of the same patient were cut and placed on plastic slides in order to carry out SEM/EDS analysis to identify the inorganic phase inside the AB, following the same methodology described in the work of Croce et al., 2013 [32]. Figure 2 shows an example of a well-developed AB: its length is about  $31\ \mu\text{m}$ , whereas the fiber diameter (measured on an area less covered by iron proteins) is about  $400\text{ nm}$ , and the protein covering shell showed a diameter ranging from  $\sim 2$  to  $\sim 2.5\ \mu\text{m}$ .

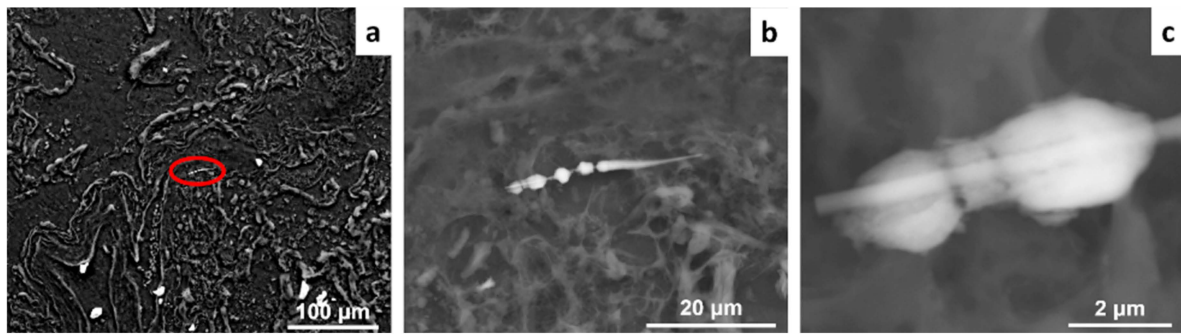


**Figure 2.** (a) Low magnification of the lung tissue; inside the circle, the position of the asbestos body is highlighted. (b) Asbestos body of (a) observed at higher magnification. (c) Magnification of the left end of the AB.

Thanks to the dimensions of the asbestos body in Figure 2, different punctual EDS analyses along lines (about 30 total lines) have been performed, and the chemicals composing the fiber could be evaluated. With respect to the study of Croce et al., 2013 [32], here the analyses were acquired both along and perpendicular to the elongation axis of the fiber, to obtain a more precise determination of the chemical elements constituting the inorganic fiber and the iron proteins. It must be considered that, in applying the described procedure, an unequivocal attribution of iron to the fiber or to the covering results is very difficult. Nevertheless, it was demonstrated that phosphorus is a component proper of the ferritin core of the proteins covering the inorganic fiber, so the identification of this chemical element might be used as a discriminating factor between the inorganic and the organic iron components, due to the fact that phosphorus is not an element composing the asbestos fibers [36,38,52]. So, it can be assumed that iron is ascribable to the inorganic fiber when P is not detected, although the obtained values are only semi-quantitative.

An example of the positions of the different analyzed points along and perpendicular to the asbestos body is shown in Figure 3, and the respective semi-quantitative obtained values are reported in Table 1.

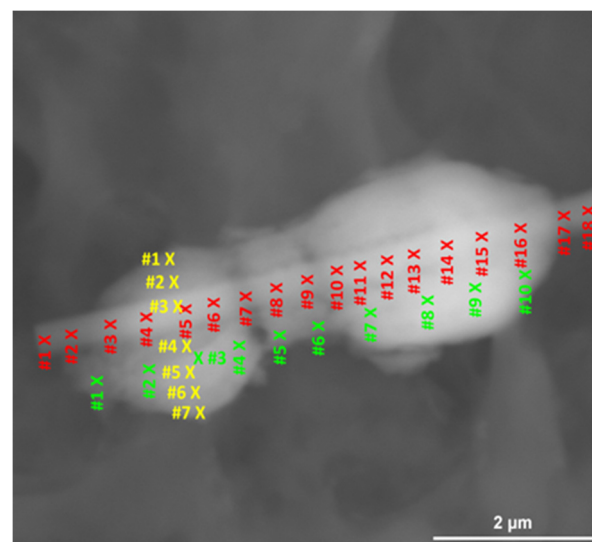


**Figure 3.** Schematization of the lines considered for the different chemical analyses, corresponding to the visible contained fiber (red points, named “line 1” in Table 1), the iron-protein covering (green points, named “line 2” in Table 1), and the data collected along a line perpendicular to the elongation axis of the fiber (yellow points, indicated as “line 3” in Table 1).

**Table 1.** Qualitative atoms % values obtained on the different points indicated in Figure 3.

	Atoms %							P/Fe Ratio
	Si	Mg	Fe	Na	Ca	S	P	
<b>Line 1</b>								
#1	0.31	0.10	0.21	0.02	0.01	0.01	0.00	0.00
#2	0.34	0.12	0.25	0.00	0.00	0.00	0.00	0.00
#3	0.31	0.15	0.44	0.00	0.00	0.00	0.00	0.00
#4	0.27	0.09	0.65	0.06	0.05	0.03	0.07	0.11
#5	0.27	0.12	0.59	0.06	0.03	0.02	0.07	0.10
#6	0.29	0.12	0.47	0.06	0.03	0.03	0.06	0.13
#7	0.29	0.12	0.50	0.06	0.03	0.02	0.07	0.10
#8	0.29	0.12	0.50	0.06	0.03	0.03	0.06	0.12
#9	0.27	0.09	0.47	0.07	0.04	0.04	0.06	0.13
#10	0.28	0.13	0.53	0.09	0.04	0.04	0.08	0.15
#11	0.26	0.10	0.63	0.06	0.04	0.03	0.09	0.14
#12	0.25	0.11	0.71	0.03	0.04	0.04	0.04	0.13
#13	0.22	0.10	0.70	0.04	0.04	0.03	0.08	0.11
#14	0.20	0.12	0.74	0.08	0.05	0.03	0.11	0.15
#15	0.20	0.10	0.66	0.07	0.03	0.02	0.09	0.14
#16	0.21	0.08	0.48	0.07	0.03	0.02	0.04	0.08
#17	0.26	0.11	0.25	0.04	0.02	0.01	0.03	0.12
#18	0.25	0.11	0.29	0.06	0.02	0.02	0.04	0.14
<b>Line 2</b>								
#1	0.04	0.05	0.31	0.03	0.05	0.01	0.05	0.16
#2	0.04	0.06	0.55	0.05	0.04	0.04	0.10	0.18
#3	0.02	0.08	0.78	0.07	0.06	0.03	0.10	0.13
#4	0.04	0.06	0.59	0.07	0.05	0.05	0.10	0.17
#5	0.06	0.05	0.21	0.07	0.04	0.04	0.04	0.19
#6	0.05	0.04	0.24	0.02	0.02	0.03	0.05	0.21
#7	0.06	0.10	0.74	0.07	0.05	0.04	0.13	0.18
#8	0.06	0.06	0.86	0.05	0.05	0.03	0.13	0.15
#9	0.05	0.04	0.83	0.07	0.05	0.04	0.13	0.16
#10	0.04	0.04	0.50	0.06	0.04	0.03	0.09	0.18
<b>Line 3</b>								
#1	0.03	0.05	0.34	0.07	0.03	0.03	0.07	0.21
#2	0.06	0.05	0.52	0.07	0.03	0.03	0.09	0.17
#3	0.20	0.11	0.60	0.05	0.04	0.03	0.06	0.10
#4	0.06	0.05	0.68	0.06	0.05	0.03	0.10	0.15
#5	0.06	0.05	0.68	0.05	0.05	0.05	0.11	0.16
#6	0.04	0.04	0.69	0.03	0.04	0.03	0.10	0.15
#7	0.04	0.05	0.62	0.08	0.06	0.04	0.09	0.15

The data reported in Table 1 show that P is not detected in the points less covered by the iron proteins. On the other hand, it has been demonstrated that this chemical element is present in the structure of the iron-protein covering, which is characterized by a structure similar to that of ferrihydrite [36,38,52]. Considering this aspect, it can be assumed that almost all the Fe detected in points #1 and #2 of line 1 in Table 1 can be ascribed to the mineral fiber. In the other analyzed points, it is impossible to attribute the iron to the inorganic or the organic phases [53–55].

In Figure 4, a schematic representation of some selected analyses acquired in the red line points in Figure 3 is reported (the numerical atoms % values are reported in line 1 in Table 1). The P peak appears less intense (or it is not detected at all) in the spectra recorded in the less covered parts of the asbestos body (spectra #1 and #2), allowing to ascribe the iron to the inorganic fiber.

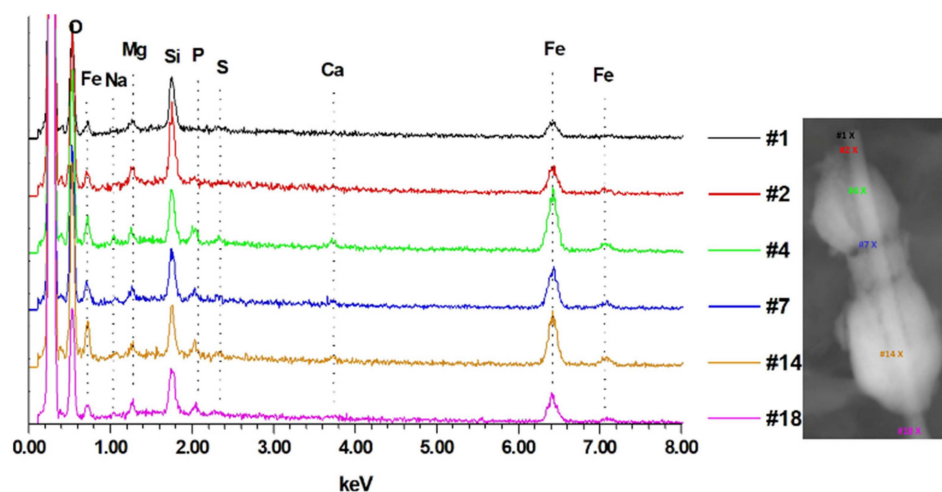


**Figure 4.** EDS spectra acquired in the points considered along the fiber. The peak relative to C is not indicated.

The different elements ascribed to inorganic components or to the biological medium, i.e., P and Ca, can be localized, but it was impossible to detect variations regarding carbon, which was always the main component in each analysis (>85% in every point, not reported in Table 1). Moreover, the SEM/EDS technique allows to qualitatively characterize the inorganic fiber inside the iron-protein coating, superimposing the spectra as described in the work of Croce et al., 2013 [32]. In fact, considering the P detected in the different analyzed points, the chemical elements ascribable to the fiber may be identified (Figure 5). In this case, the superimposed spectra are three: the spectrum obtained analyzing a point where only the iron-protein coating is present (analysis #3 in line 2, grey in Figure 5), a second one recorded on a less covered area of the fiber (analysis #1 in line 1, black in Figure 5), and a third one where the two components (protein and fiber, analysis #10 in line 1, orange in Figure 5) were recognizable.

As can be seen in Figure 5, iron is a component proper of the fiber (black line in Figure 5), with these peaks appearing with lower intensity with respect to the ones observed when the protein component (grey and orange in Figure 5) is present. Iron peaks show higher intensity in spectra recorded where fiber and protein components are present (analysis #10 of line 1 in Figure 5). Considering the data recorded on this asbestos body, the inorganic fiber is composed of Si > Mg > Fe in decreasing amounts, so it may be ascribed to the asbestos phase “anthophyllite”.

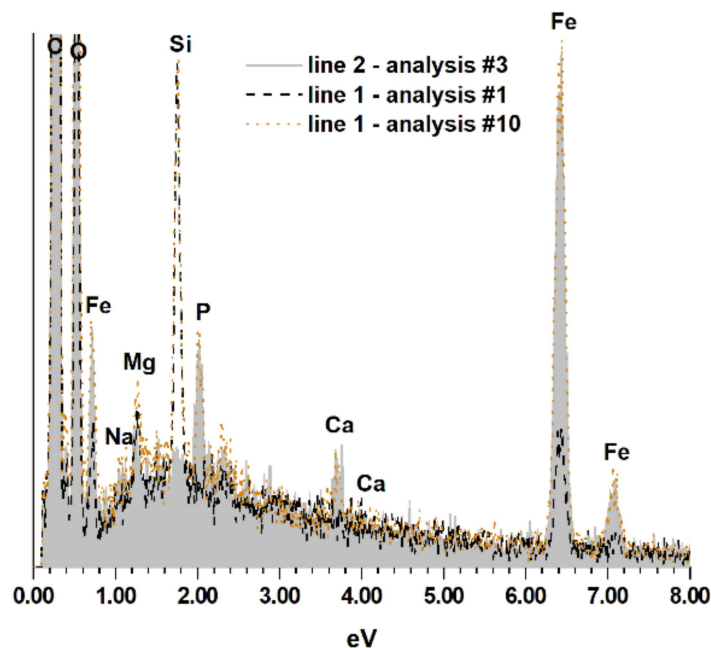


**Figure 5.** EDS superimposition of three spectra obtained on the iron-protein covering (grey), the less covered portion of the fiber (black), and the area where the fiber is more embedded by the organic component (orange).

In addition to OM and SEM analyses, ABs observed in the lung section of the same patient have been characterized under micro-Raman spectroscopy, in order to characterize not only the iron covering but also to evaluate the presence of carbonaceous phases, “unidentifiable” in the SEM/EDS analyses. The laser beam was addressed onto areas appearing most covered by iron proteins during OM and SEM observations.

In Figure 6, an example of AB, observed under the OM annexed to the Raman spectroscope (80X objective), is reported. In this case, subsequent acquisitions on the more covered portion of the fiber were carried out, considering the 1800–100  $\text{cm}^{-1}$  spectral range. The applied method was the same as that described in the work of Rinaudo et al., 2010 [49], where only the spectral range of 1200–200  $\text{cm}^{-1}$  was considered. So, recognition of both inorganic and organic phases may be carried out taking into account the spectral range considered in this work. The 1800–100  $\text{cm}^{-1}$  range was chosen to obtain well-resolved spectra and to define after how much time the band features were changing during acquisition, to understand if mapping analyses were able to give results preventing sample modifications.

Figure 6 shows spectral features evolution in the subsequent spectra. In the analyses carried out during the first ~30 min, the most prominent bands are related to carbonaceous material (CM) [34,35]. In the spectra recorded after this time, the bands related to the organic component decrease in intensity, and an increase in the intensities of the bands related to iron oxides is detected (see Discussion section for more details). Moreover, the bands related to these last phases show an evolution also in Raman shifts, up to a feature ascribable to the iron oxide “hematite”,  $\text{Fe}_2\text{O}_3$ , and the disappearing of signals related to carbon phases can be observed: note that the band lying at about 1300  $\text{cm}^{-1}$  is ascribed to the second order of the iron oxide phase when CMs are not detected.

As it concerns CM Raman bands, a fitting procedure was applied in the 1800–800  $\text{cm}^{-1}$  spectral range, considering the six bands indicated in the Materials and Methods section; the results are reported in Figure 7. In the analyzed case, the intensities of the two Raman bands are 109.28 (a.u., D1 band) and 75.54 (a.u., G band), giving an  $R_1$  ratio of 1.45. This value indicates a disordered structure of the CMs on the asbestos body, with a ratio similar to the ones obtained from CMs observed on crocidolite fiber surfaces [34]. The values of intensities of D1 and G bands observed in the other ten representative spectra- and their

relative  $R_1$  ratios—from CMs on ABs observed inside the same histological sample—are reported in Table 2.

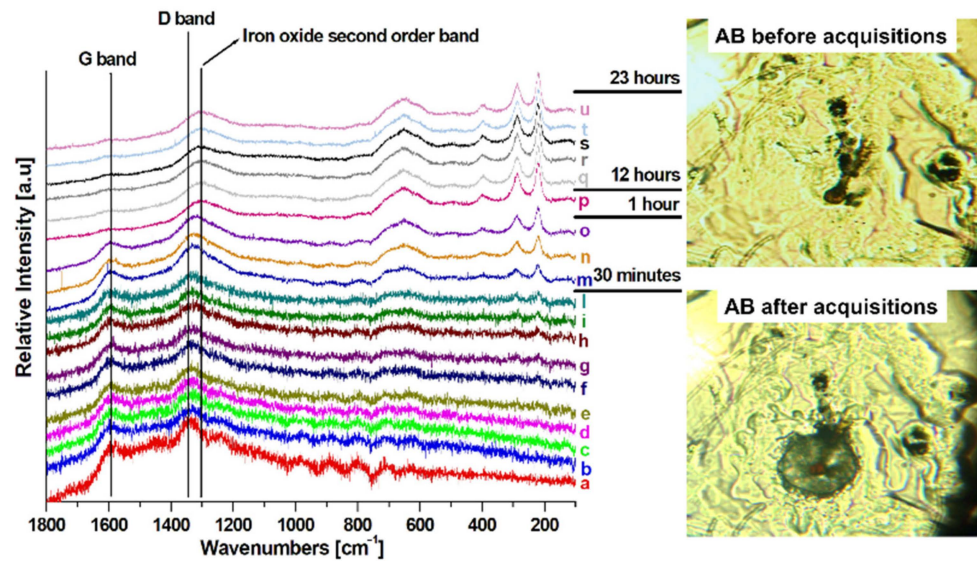


**Figure 6.** Example of subsequent (“a” is the first analysis, “u” the last one) Raman analysis carried out on the asbestos body reported on the right. Shown is the asbestos body before and after the cycle of analysis.

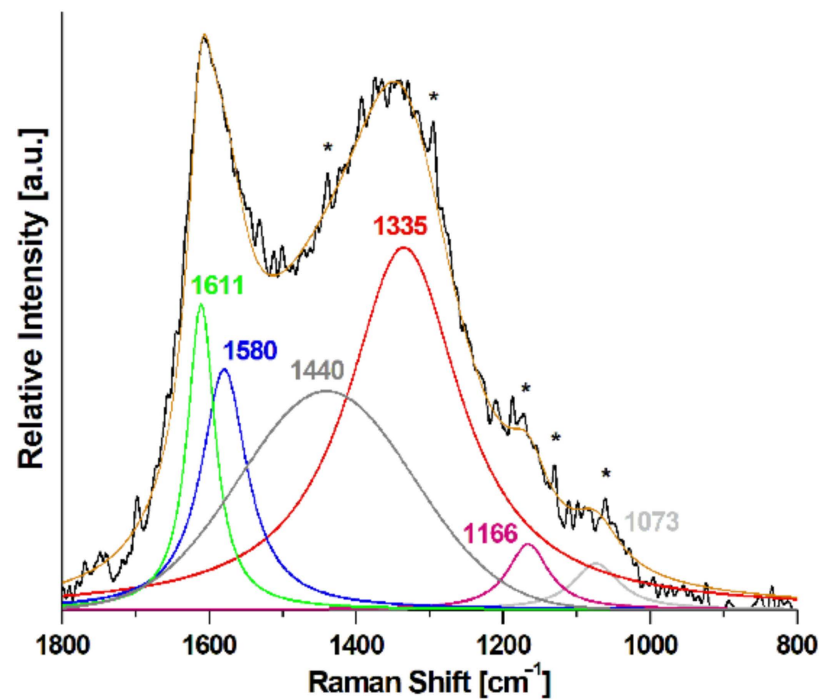


**Figure 7.** Fitting on a Raman spectrum obtained by analyzing the AB covering. The various colors indicate the different bands: G in blue, D1 in red, D2 in green, D3 in dark gray, D4 in pink, and D5 in light gray. The bands indicated by \* are ascribed to the paraffin embedding in the lung tissue [56].

**Table 2.** Observed intensities of D1 and G bands in ten representative spectra and their calculated  $R_1$  ratios.

	D1 Band Intensity	G Band Intensity	$R_1$ Ratio
Spectrum #1	272.12	188.97	1.44
Spectrum #2	154.78	108.24	1.43
Spectrum #3	150.93	101.29	1.49
Spectrum #4	159.03	109.68	1.45
Spectrum #5	177.60	121.64	1.46
Spectrum #6	169.23	116.71	1.45
Spectrum #7	154.56	108.84	1.42
Spectrum #8	148.96	104.90	1.42
Spectrum #9	143.57	99.70	1.44
Spectrum #10	145.97	99.98	1.46

As can be observed in Table 2, the  $R_1$  ratio shows a mean value of 1.44, with a maximum value of 1.49 and a minimum of 1.42, so the order degree of the analyzed CMs is comparable.

Starting from these results, it was possible to set up the instrument configuration and parameters in order to obtain spectra without modifying (morphologically and chemically) the analyzed ABs. Raman mappings were therefore carried out on different covered fibers. In Figure 8, a Raman mapping on a well-developed formation is reported.

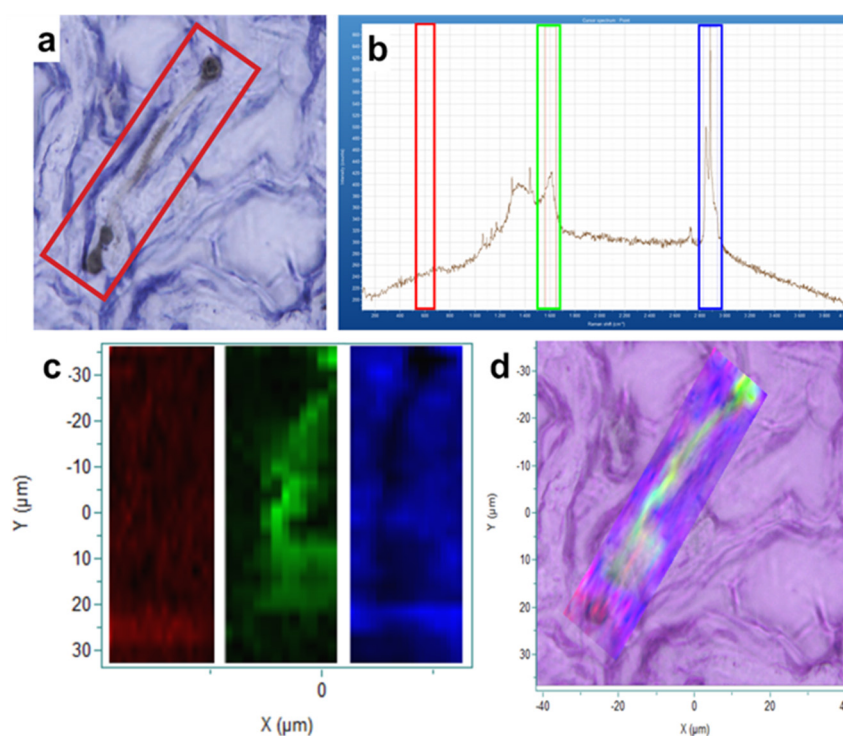


**Figure 8.** (a) Asbestos body in lung observed by OM; the red rectangle indicates the area analyzed during Raman mapping. (b) Positions of the bands considered for Raman mapping (red = bands related to silicate phase; green = CMs; blue = tissue + paraffin). (c) Mapping of the bands reported in (b); (d) Superimposition of the mapping on the OM photograph.

Three Raman spectral ranges were considered for map generation: (i)  $\sim 550\text{--}700\text{ cm}^{-1}$ , where the Si-O-Si symmetric stretching bands lie (in red in Figure 8) for the silicate compo-

nent; (ii)  $\sim 1500\text{--}1650\text{ cm}^{-1}$ , where the G and D2 bands of the CMs are observed (green in Figure 8); (iii)  $\sim 2700\text{--}3000\text{ cm}^{-1}$ , to collect the map relative to the paraffin wax embedding the tissue (blue in Figure 8).

From the green map in Figure 8c, it is evident the presence of a carbonaceous covering, adhered to the iron protein capsule embedding the fiber. As it concerns the recognition of the silicatic component inside the asbestos body, it is difficult to assign the mineral phase to it. In fact, only in a very small portion of the corpuscle is it possible to observe very weak signals, which are more visible only after the superimposition of the three Raman maps (see Figure 8d).

#### 4. Discussion

In this work, two complementary techniques—SEM/EDS and micro-Raman spectroscopy—were applied to the characterization of the components constituting the typical marker for asbestos exposure, the “asbestos bodies”. As specified before, SEM/EDS allows the collection of spectra relative to the chemical components constituting the different areas of the observed sample, whereas Raman spectroscopy allows to obtain information related to the chemical bonds of the analyzed materials. The development of a methodology that allows the identification of not only the inorganic components but also the relationships between biological and inorganic components, without removing the tissues, may be very important to understanding the mechanisms of fiber pathogenicity.

In fact, manipulation procedures for the extraction of the asbestos fibers or bodies are often necessary with the consequent risk of losing the biological material (e.g.: during tissue digestion or ashing), altering both the chemical composition and the structure of ABs [37]. So, in the field of medical geology, it is really important to develop a method allowing the characterization of ABs directly inside the tissues, to maintain unaltered these formations and their relationships with the organic matrices.

In this work, SEM/EDS and micro-Raman spectroscopy were applied to histological samples routinely analyzed by pathologists to better define the inorganic and the organic components compared to the past works [32,49]. In fact, compared to [32], iron has been deeply characterized, to define if it was possible to distinguish the inorganic component from the organic one. Moreover, compared to [49], also analyzed was the Raman range where the first-order bands of CMs lie, which were analyzed only in raw asbestos in previous works [34,35], to determine if also these phases were identifiable directly in histological sections.

As it concerns the SEM/EDS technique, in the operative conditions applied in this work, only qualitative data could be obtained: nevertheless, it was possible to distinguish the mineral phase by comparing the obtained data to the reference spectra previously collected on pure samples.

Considering the organic component, due to the value of detected carbon (a mean  $> 85\%$ ), it was not possible to extrapolate information about the presence of CMs or other organic components adhered to the asbestos fibers. Nevertheless, observing the data relative to the iron element, it could be related to the organic or the inorganic phases: in fact, when phosphorus was detected, it can be ascribed to the iron-protein covering, due to the strict relationship between these two chemical elements, whereas it is attributed to the silicatic phase when P was not detected. In fact, it has been demonstrated that phosphorous can be adsorbed on fiber surfaces during amphibole transformation in contact with tissues [38], and it is detected mainly inside the protein coating [36]. In the present work, it was possible to obtain the same result observed by Avramescu et al., 2023 [36], without the removal of the biological component.

It has been demonstrated that SEM/EDS is very useful for mineral recognition also when the fiber is embedded inside iron-protein coverings. Considering the distribution of phosphorus in the ABs, it is also possible to exclude the detected iron from the chemical composition of the mineral phase. Phosphorus presence in chemical composition might be useful to better identify the mineral phase associated with the fibrous morphologies,

principally in a qualitative analysis, when the fiber is composed also of iron (e.g.: amosite-anthophyllite, actinolite-ferroactinolite, etc.). On the other hand, no information about the other organic components can be obtained.

Micro-Raman spectroscopy is another technique that allows the collection of data from ABs directly inside the biological medium, maintaining the relationships between the inorganic and the organic components. When the laser beam gives too much energy, the iron contained inside the protein cores tends to reorganize its structure until the formation of the mineral hematite—chemical formula  $\text{Fe}_2\text{O}_3$ . Its formation is related to the degradation of CM particles adhered to the covering surface: in fact, collecting subsequent spectra on the same point of the asbestos body, it was possible to observe the disappearing of the D and G bands ascribed to the carbonaceous component in relation to the increasing intensity of the Raman bands ascribed to the iron oxide phase.

This tendency is more frequent in asbestos bodies more covered by carbonaceous material: from the optical point of view, the covering level is associable with a darker color (i.e.: dark red or brown) of the morphology.

Applying a fitting procedure to evaluate the numerical parameters of the different bands lying in the range of  $800\text{--}1800\text{ cm}^{-1}$ , it is possible to determine the order degree of the observed carbonaceous materials. In future studies, it might be interesting to evaluate the order degree of these particles in different patients, to determine if the Raman spectra of the organic material can be useful to obtain information about the organic components on the fiber surfaces after interaction with lung tissues.

For example, Avramescu et al., 2023 [36], observed that iron-protein covering was denser in smokers, whereas there were different concentric rings in non-smokers, suggesting a more variable iron supply in AB formation. This study was carried out using SEM, focused ion beam (FIB), and transmission electron microscopy (TEM) after digestion of the tissues. A future application of micro-Raman spectroscopy to a set of samples deriving from smokers and non-smokers might improve the understanding of these structures from another point of view, with the advantage that the analyses can be performed directly inside the tissues, preventing the loss of information about the particles adhered to AB surfaces.

It must be considered that carbon black is listed as a group 2B carcinogen by the IARC [57], and it is related to an increase in lung cancer risk [58–60], so detection and localization of CMs related to asbestos fibers may be useful for future studies concerning the comprehension of cancer development in terms of synergistic effects.

Moreover, micro-Raman spectroscopy demonstrated its advantages also in mapping analyses, allowing the operator to understand where the different organic or inorganic phases are localized in the asbestos bodies. No well-developed Raman spectra of the mineral phase contained in the embedding were recorded: it may be due to the iron coating signal or to the loss of mineral structure undergone by the fiber. This point must be deepened in future studies.

In conclusion, the coupling of SEM/EDS and micro-Raman spectroscopy allows us to obtain information about the mineral phases contained inside the asbestos bodies and the other pollutants next to them, as carbonaceous materials, thanks to the direct analysis in the tissues, without particular manipulations. In the future, it might be interesting to apply these non-destructive techniques to a greater number of cases (or to samples with known exposures, as it is carried out in *in vitro* and *in vivo* studies), trying to provide some results that are useful to better understand what happens to the different inhaled (or also ingested) particles and fibers when they come in contact with the tissues. Moreover, it may be interesting to apply these techniques to different cohorts of patients exposed to different inorganic and organic pollutants, or to smoking and non-smoking patients, to observe whether differences in AB structures are identifiable.

In this way, the collaboration of the mineralogist with researchers of other biological and medical fields might improve the knowledge of the different respiratory and extra-respiratory diseases, considering them from the point of view of interdisciplinary studies in medical geology.

**Author Contributions:** Conceptualization, A.C. (Alessandro Croce); methodology, A.C. (Alessandro Croce); software, A.C. (Alessandro Croce); validation, C.R. and A.C. (Alessandro Croce); formal analysis, A.C. (Alessandro Croce); investigation, A.C. (Alessandro Croce); resources, C.R.; data curation, A.C. (Alessandro Croce); writing—original draft preparation, A.C. (Alessandro Croce), D.B., A.C. (Antonio Calisi), G.G. and C.R.; writing—review and editing, C.R., D.B. and A.C. (Alessandro Croce); visualization, A.C. (Alessandro Croce) and L.C.; supervision, C.R., M.B. and A.M.; project administration, A.C. (Alessandro Croce); funding acquisition, C.R. All authors have read and agreed to the published version of the manuscript.

**Funding:** This research received no external funding.

**Institutional Review Board Statement:** The study was conducted according to the guidelines of the Declaration of Helsinki, and approved by the Ethics Committees of the University of Torino (Turin, Italy) and of the Martini hospital (Turin, Italy) Ethical Committee of ASL TO2 (no. 38851 (protocol code 38851 on 29 July 2013).

**Data Availability Statement:** Data is contained within the article.

**Acknowledgments:** This work was supported by UPO (“Integrated system for the fibre pollution assessment in air and characterization of the fibrous phases in different matrixes”). The authors wish to thank the Editors and the anonymous referees for their work.

**Conflicts of Interest:** The authors declare no conflicts of interest.

## References

1. International Agency for Research on Cancer (IARC). Asbestos (chrysotile, amosite, crocidolite, tremolite, actinolite, and anthophyllite). In *IARC Monographs on the Evaluation of Carcinogenic Risks to Humans*; IARC: Lyon, France, 2012; Volume 100C, pp. 219–309. ISBN 978-92-832-1320-8.
2. Italian Government. Legislative Decree No. 277 of 15 August 1991, Implementing EU Directives No. 80/1107/EEC, No. 82/605/EEC, No. 83/477/EEC, No. 86/188/EEC, and No. 88/642/EEC, on the Protection of Workers from the Risks Related to Exposure to Chemical, Physical and Biological Agents at Work. In *Gazzetta Ufficiale Supplemento Ordinario No. 200*; Italian Government: Rome, Italy, 1991.
3. Hawthorne, F.C.; Oberti, R.; Harlow, G.E.; Maresch, W.V.; Martin, R.F.; Schumacher, J.C.; Welch, M.D. Nomenclature of the amphibole supergroup. *Am. Mineral.* **2012**, *97*, 2031–2048. [[CrossRef](#)]
4. Leake, B.E.; Woolley, A.R.; Arps, C.E.S.; Birch, W.D.; Gilbert, M.C.; Grice, J.D.; Hawthorne, F.C.; Kato, A.; Kisch, H.J.; Krivovichev, V.G.; et al. Nomenclature of amphiboles: Report of the Subcommittee on amphiboles of the International Mineralogical Association, Commission on New Minerals and Mineral Names. *Can. Mineral.* **1997**, *35*, 219–246.
5. Whittaker, E.J.W.; Zussman, J. The characterization of serpentine minerals by X-ray diffraction. *Mineral. Mag.* **1956**, *233*, 107–126. [[CrossRef](#)]
6. Bartrip, P.W.J. History of asbestos related disease. *Postgrad. Med. J.* **2004**, *80*, 72–76. [[CrossRef](#)]
7. Donaldson, K.; Seaton, A. A short history of the toxicology of inhaled particles. *Part. Fibre Toxicol.* **2012**, *9*, 13. [[CrossRef](#)] [[PubMed](#)]
8. Caraballo-Arias, Y.; Rocuzzo, F.; Graziosi, F.; Danilevskaia, N.; Rota, S.; Zunarelli, C.; Caffaro, P.; Boffetta, P.; Bonetti, M.; Violante, F.S. Quantitative assessment of asbestos fibers in abdominal organs: A scoping review. *Med. Lav.* **2023**, *114*, e2023048.
9. Porzio, A.; Feola, A.; Parisi, G.; Lauro, A.; Campobasso, C.P. Colorectal cancer: 35 cases in asbestos-exposed workers. *Healthcare* **2023**, *11*, 3077. [[CrossRef](#)]
10. Brandi, G.; Straif, K.; Mandrioli, D.; Curti, S.; Mattioli, S.; Tavolari, S. Exposure to asbestos and increased intrahepatic cholangiocarcinoma risk: Growing evidences of a putative causal link. *Ann. Glob. Health* **2022**, *88*, 41. [[CrossRef](#)]
11. Grosso, F.; Croce, A.; Libener, R.; Mariani, N.; Pastormerlo, M.; Maconi, A.; Rinaudo, C. Asbestos fiber identification in liver from cholangiocarcinoma patients living in an asbestos polluted area: A preliminary study. *Tumori J.* **2019**, *105*, 404–410. [[CrossRef](#)]
12. Gamble, J.F. Asbestos and colon cancer: A weight-of-the-evidence review. *Environ. Health Perspect.* **1994**, *102*, 1038–1050. [[CrossRef](#)]
13. Ehrlich, A.; Rohl, A.N.; Holstein, E.C. Asbestos bodies in carcinoma of colon in an insulation worker with asbestosis. *JAMA* **1985**, *254*, 2932–2933. [[CrossRef](#)]
14. Ehrlich, A.; Gordon, R.E.; Dikman, S.H. Carcinoma of the colon in asbestos-exposed workers: Analysis of asbestos content in colon tissue. *Am. J. Ind. Med.* **1991**, *19*, 629–636. [[CrossRef](#)]
15. Kobayashi, H.; Ming, Z.W.; Watanabe, H.; Ohnishi, Y. A quantitative study on the distribution of asbestos bodies in extrapulmonary organs. *Acta Pathol. Jpn.* **1987**, *37*, 375–383. [[CrossRef](#)]
16. Barrett, J.C.; Lamb, P.W.; Wiseman, R.W. Multiple mechanisms for the carcinogenic effects of asbestos and other mineral fibers. *Environ. Health Perspect.* **1989**, *81*, 81–89. [[CrossRef](#)]

17. Wachowski, L.; Domka, L. Sources and effects of asbestos and other mineral fibres present in ambient air. *Pol. J. Environ. Stud.* **2000**, *9*, 443–454.
18. Andolfi, L.; Trevisan, E.; Zweyer, M.; Prato, S.; Troian, B.; Vita, F.; Borelli, V.; Soranzo, M.R.; Melato, M.; Zabucchi, G. The crocidolite fiber interaction with human mesothelial cells as investigated by combining electron microscopy, atomic force and scanning near-field optical microscopy. *J. Microsc.* **2013**, *249*, 173–183. [[CrossRef](#)]
19. Aust, A.E.; Cook, P.M.; Dodson, R.F. Morphological and chemical mechanisms of elongated mineral particle toxicities. *J. Toxicol. Environ. Health Part B* **2011**, *14*, 40–75. [[CrossRef](#)]
20. Carbone, M.; Ly, B.H.; Dodson, R.F.; Pagano, I.; Morris, P.T.; Dogan, U.A.; Gazdar, A.F.; Pass, H.I.; Yang, H. Malignant mesothelioma: Facts, myths, and hypotheses. *J. Cell. Physiol.* **2012**, *227*, 44–58. [[CrossRef](#)]
21. Crawford, D. Electron microscopy applied to studies of the biological significance of defects in crocidolite asbestos. *J. Microsc.* **1980**, *120*, 181–192. [[CrossRef](#)]
22. Fubini, B.; Mollo, L. Role of iron in the reactivity of mineral fibers. *Toxicol. Lett.* **1995**, *82–83*, 951–960. [[CrossRef](#)]
23. Goodglick, L.A.; Kane, A.B. Cytotoxicity of long and short crocidolite asbestos fibers in vitro and in vivo. *Cancer Res.* **1990**, *50*, 5153–5163.
24. Hearne, G.R.; Kolk, B.; Pollak, H.; van Wyk, J.A.; Gulumian, M. Bulk and surface modifications in detoxified crocidolite. *J. Inorg. Biochem.* **1993**, *50*, 145–156. [[CrossRef](#)]
25. Martra, G.; Chiardola, E.; Coluccia, S.; Marchese, L.; Tomatis, M.; Fubini, B. Reactive sites at the surface of crocidolite asbestos. *Langmuir* **1999**, *15*, 5742–5752. [[CrossRef](#)]
26. Mossman, B.; Light, W.; Wei, E. Asbestos: Mechanisms of toxicity and carcinogenicity in the respiratory tract. *Annu. Rev. Pharmacol.* **1983**, *23*, 595–615. [[CrossRef](#)] [[PubMed](#)]
27. Pacella, A.; Fantauzzi, M.; Turci, F.; Cremisini, C.; Montereali, M.R.; Nardi, E.; Atzei, D.; Rossi, A.; Andreozzi, G.B. Dissolution reaction and surface iron speciation of UICC crocidolite in buffered solution at pH 7.4: A combined ICP-OES, XPS and TEM investigation. *Geochim. Cosmochim. Acta* **2014**, *127*, 221–232. [[CrossRef](#)]
28. Rihn, B.; Coulais, C.; Kauffer, E.; Bottin, M.C.; Martin, P.; Yvon, F.; Vigneron, J.C.; Binet, S.; Monhoven, N.; Steiblen, G.; et al. Inhaled crocidolite mutagenicity in lung DNA. *Environ. Health Perspect.* **2000**, *108*, 341–346. [[CrossRef](#)] [[PubMed](#)]
29. Wagner, J.C.; Berry, G.; Timbrell, V. Mesotheliomata in rats after inoculation with asbestos and other materials. *Br. J. Cancer* **1973**, *28*, 173–185. [[CrossRef](#)] [[PubMed](#)]
30. Wagner, J.C.; Griffiths, D.M.; Hill, R.J. The effect of fiber size on the in vivo activity of UICC crocidolite. *Br. J. Cancer* **1984**, *49*, 453–458. [[CrossRef](#)]
31. Werner, A.J.; Hochella, M.F., Jr.; Guthrie, G.D.; Hardy, J.A.; Aust, A.E.; Rimstidt, J.D. Asbestiform riebeckite (crocidolite) dissolution in presence of Fe chelators: Implications for mineral-induced disease. *Am. Mineral.* **1995**, *80*, 1093–1103. [[CrossRef](#)]
32. Croce, A.; Musa, M.; Allegrina, M.; Trivero, P.; Rinaudo, C. Environmental scanning electron microscopy technique to identify asbestos phases inside ferruginous bodies. *Microsc. Microanal.* **2013**, *19*, 420–424. [[CrossRef](#)] [[PubMed](#)]
33. Musa, M.; Croce, A.; Allegrina, M.; Rinaudo, C.; Belluso, E.; Bellis, D.; Toffalorio, F.; Veronesi, G. The use of Raman spectroscopy to identify inorganic phases in iatrogenic pathological lesions of patients with malignant pleural mesothelioma. *Vib. Spectrosc.* **2012**, *61*, 66–71. [[CrossRef](#)]
34. Croce, A.; Arrais, A.; Rinaudo, C. Raman micro-spectroscopy identifies carbonaceous particles lying on the surface of crocidolite, amosite, and chrysotile fibers. *Minerals* **2018**, *8*, 249. [[CrossRef](#)]
35. Rinaudo, C.; Croce, A. Micro-Raman spectroscopy, a powerful technique allowing sure identification and complete characterization of asbestiform minerals. *Appl. Sci.* **2019**, *9*, 3092. [[CrossRef](#)]
36. Avramescu, M.L.; Potiszil, C.; Kunihiro, T.; Okabe, K.; Nakamura, E. An investigation of the internal morphology of asbestos ferruginous bodies: Constraining their role in the onset of malignant mesothelioma. *Part. Fibre Toxicol.* **2023**, *20*, 19. [[CrossRef](#)] [[PubMed](#)]
37. Bardelli, F.; Giacobbe, C.; Ballirano, P.; Borelli, V.; Di Benedetto, F.; Montegrassi, G.; Bellis, D.; Pacella, A. Closing the knowledge gap on the composition of the asbestos bodies. *Environ. Geochem. Health* **2023**, *45*, 5039–5051. [[CrossRef](#)] [[PubMed](#)]
38. Vigliaturo, R.; Jannik, M.; Dražić, G.; Podobnik, M.; Tušek Žnidarič, M.; Della Ventura, G.; Redhammer, G.J.; Žnidarič, N.; Caserman, S.; Gieré, R. Nanoscale transformations of amphiboles within human alveolar epithelial cells. *Sci. Rep.* **2022**, *12*, 1782. [[CrossRef](#)]
39. Croce, A.; Allegrina, M.; Rinaudo, C.; Gaudino, G.; Yang, H.; Carbone, M. Numerous iron-rich particles lie on the surface of erionite fibers from Rome (Oregon, USA) and Karlik (Cappadocia, Turkey). *Microsc. Microanal.* **2015**, *21*, 1341–1347. [[CrossRef](#)] [[PubMed](#)]
40. Bowes, D.R.; Farrow, C.M. Major and trace element compositions of the UICC standard asbestos samples. *Am. J. Ind. Med.* **1997**, *32*, 592–594. [[CrossRef](#)]
41. Burns, R.G.; Prentice, F.J. Distribution of iron cations in the crocidolite structure. *Am. Mineral.* **1968**, *53*, 770–776.
42. Galumian, M.; Pollak, H. Effect of microwave radiation on surface charge, surface sites and ionic state of iron, and the activity of crocidolite asbestos fibres. *Hyperfine Interact.* **1998**, *111*, 291–298. [[CrossRef](#)]
43. Graham, A.; Higinbotham, J.; Doug, A.; Donaldson, K.; Beswick, P.H. Chemical differences between long and short amosite asbestos: Differences in oxidation state and coordination sites of iron, detected by infrared spectroscopy. *Occup. Environ. Med.* **1999**, *56*, 606–611. [[CrossRef](#)]

44. Gunter, M.E.; Sanchez, M.S.; Williams, T.J. Characterization of chrysotile samples for the presence of amphiboles: The Carey Canadian deposit, Southeastern Quebec, Canada. *Can. Mineral.* **2007**, *45*, 263–280. [[CrossRef](#)]
45. Hilborn, J.J.; Thomas, R.S.; Lao, R.C. The organic content of the international reference samples of asbestos. *Sci. Total Environ.* **1974**, *3*, 129–140. [[CrossRef](#)]
46. Harington, J.S. Chemical studies of asbestos. *Ann. N. Y. Acad. Sci.* **1965**, *132*, 31–47. [[CrossRef](#)]
47. Steel, E.B.; Small, J.A. Accuracy of transmission electron microscopy for the analysis of asbestos in ambient environments. *Anal. Chem.* **1985**, *57*, 209–213. [[CrossRef](#)]
48. Platek, S.F.; Riley, R.D.; Simon, S.D. The classification of asbestos fibers by scanning electron microscopy and computer-digitizing tablet. *Ann. Occup. Hyg.* **1992**, *36*, 155–171. [[PubMed](#)]
49. Rinaudo, C.; Croce, A.; Musa, M.; Fornero, E.; Allegrina, M.; Trivero, P.; Bellis, D.; Sferch, D.; Toffalorio, F.; Veronesi, G.; et al. Study of inorganic particles, fibers, and asbestos bodies by variable pressure scanning electron microscopy with annexed energy dispersive spectroscopy and micro-Raman spectroscopy in thin sections of lung and pleural plaque. *Appl. Spectrosc.* **2010**, *64*, 571–577. [[CrossRef](#)] [[PubMed](#)]
50. Prashanth, M.; Verma, O. Medical geology: An interdisciplinary approach intended to unfold the issues of natural environment on public health. *J. Geosci. Res.* **2022**, *7*, 139–144. [[CrossRef](#)]
51. Croce, A.; Re, G.; Bisio, C.; Gatti, G.; Coluccia, S.; Marchese, L. On the correlation between Raman spectra and structural properties of activated carbons derived by hyper-crosslinked polymers. *Res. Chem. Intermed.* **2021**, *47*, 419–431. [[CrossRef](#)]
52. Chasteen, N.D.; Harrison, P.M. Mineralization in ferritin: An efficient means of iron storage. *J. Struct. Biol.* **1999**, *126*, 182–194. [[CrossRef](#)]
53. Harrison, P.M.; Fischbach, F.A.; Hoy, T.G.; Haggis, G.H. Ferric oxyhydroxide core of ferritin. *Nature* **1967**, *216*, 1188–1190. [[CrossRef](#)] [[PubMed](#)]
54. St. Pierre, T.G.; Kim, K.S.; Webb, J.; Mann, S.; Dickson, D.P.E. Biomineralization of iron: Mossbauer spectroscopy and electron microscopy of ferritin cores from the chiton *Acanthopleura hirtosa* and the limpet *Patella laticostata*. *Inorg. Chem.* **1990**, *29*, 1870–1874. [[CrossRef](#)]
55. Wade, V.J.; Treffry, A.; Laulhere, J.P.; Bauminger, E.R.; Cleton, M.I.; Mann, S.; Briat, J.F.; Harrison, P.M. Structure and composition of ferritin cores from pea seed (*Pisum sativum*). *Biophys. Biochim. Acta* **1993**, *1161*, 91–96. [[CrossRef](#)]
56. Mian, S.A.; Colley, H.E.; Thornhill, M.H.; Rehman, I.U. Development of a dewaxing protocol for tissue-engineered models of the oral mucosa used for Raman spectroscopic analysis. *Appl. Spectrosc. Rev.* **2014**, *49*, 614–617. [[CrossRef](#)]
57. International Agency for Research on Cancer (IARC). Carbon black, titanium dioxide, and talc. In *IARC Monographs on the Evaluation of Carcinogenic Risks to Humans*; IARC: Lyon, France, 2010; Volume 93, pp. 43–192. ISBN 978-92-832-1293-5.
58. Zhang, J.; Li, X.; Cheng, W.; Li, Y.; Shi, T.; Jiang, Y.; Wang, T.; Wang, H.; Ren, D.; Zhang, R.; et al. Chronic carbon black nanoparticle exposure increases lung cancer risk by affecting the cell cycle via circulatory inflammation. *Environ. Pollut.* **2022**, *305*, 119293. [[CrossRef](#)] [[PubMed](#)]
59. Lequy, E.; Siemiatycki, J.; de Hoogh, K.; Vienneau, D.; Dupuy, J.F.; Garès, V.; Hertel, O.; Christensen, J.H.; Goldberg, M.; Zins, M.; et al. Contribution of long-term exposure to outdoor black carbon to the carcinogenicity of air pollution: Evidence regarding risk of cancer in the Gazel Cohort. *Environ. Health Perspect.* **2021**, *129*, 37005. [[CrossRef](#)]
60. Grahame, T.J.; Klemm, R.; Schlesinger, S.B. Public health and components of particulate matter: The changing assessment of black carbon. *J. Air Waste Manag.* **2014**, *64*, 620–660. [[CrossRef](#)]

**Disclaimer/Publisher’s Note:** The statements, opinions and data contained in all publications are solely those of the individual author(s) and contributor(s) and not of MDPI and/or the editor(s). MDPI and/or the editor(s) disclaim responsibility for any injury to people or property resulting from any ideas, methods, instructions or products referred to in the content.